RSC Advances

PAPER

View Article Online
View Journal | View Issue



Cite this: *RSC Adv.*, 2023, **13**, 29231

# Robust and facile detection of formaldehyde through transition metals doped olympicene sensors: a step forward DFT investigation†

Muhammad Aetizaz,[a] Faizan Ullah,[a] Sehrish Sarfaraz,[a] Tariq Mahmood[b] and Khurshid Ayub *[a]

Formaldehyde, a volatile organic compound (VOC) released by building and decoration materials, has many applications in the chemical feedstock industry. Excessive release of formaldehyde can cause serious health issues, such as chest tightness, cough, cancer, and tissue damage. Therefore, detection of formaldehyde is required. Herein transition metal (Fe, Ni, and Pd) doped olympicene is evaluated as a gas sensor for the detection of formaldehyde. The performance of the designed electrochemical sensor is evaluated through interaction energy, natural bond orbital (NBO) non-covalent interaction (NCI), electron density differences (EDD), electrostatic potential (ESP), quantum theory of atom in molecule (QTAIM), frontier molecular orbital (FMO), and density of states (DOS) analysis. Interaction energies obtained at B3LYP-D3/def-2 TZVP level of theory shows that formaldehyde is physiosorbed over the surface of transition metal doped olympicene. The trend for interaction energy is OLY(Ni)/HCHO > OLY(Fe)/HCHO > OLY(Pd)/HCHO. The presence of non-covalent interactions is confirmed by the QTAIM and NCI analyses, while transfer of charges is confirmed by natural bond orbital analysis. The reduced density gradient (RDG) approach using noncovalent interaction (NCI) analysis demonstrates that electrostatic hydrogen bonding interactions prevail in the complexes. Recovery time is calculated to check the reusability of the sensor. This study may provide a deep insight for the designing of highly efficient electrochemical sensor against formaldehyde with transition metals doped on olympicene.

Received 15th June 2023
Accepted 21st September 2023

DOI: 10.1039/d3ra04019d

rsc.li/rsc-advances



## 1 Introduction

Environmental imbalance due to increasing air pollution has many harmful effects on aquatic and marine life.[1] Numerous gases that are present on the earth's surface are crucial for earth's environment. Initially these were present in balanced amount but, due to many factors like sudden increase in population, industrialization, transportation, and most important human activities, an imbalance is created to the environment.[2] Gases containing carbon, nitrogen, sulfur, and volatile organic compounds have major contributions in polluting the environment. Apart from all these gases formaldehyde is a dangerous volatile organic compound (VOC), released by building structures and decoration materials.[3] Almost 90% of formaldehyde is produced by the physiochemical reactions in the exosphere of the atmosphere.[4] Moreover, as far as its production is concerned it is also produced by the combustion of methane and many other organic compounds. Formaldehyde has been frequently employed by organic chemists to make resins including phenol-formaldehyde, urea-formaldehyde, melamine, polyoxymethylene plastics, and methylene diphenyl diisocyanate because of its adhesive characteristics.[5] Excessive inhalation of formaldehyde at amounts higher than 0.1 ppm from indoor objects like cement, furniture *etc.*, may cause severe health complications.[6] It is also known as harmful indoor killer due to its harsh effects on humans health including respiratory problems and certain death due to cancer.[7] Long exposure of formaldehyde can cause chest tightness, cough, asthma, throat problems and eye irritation.[8] Another important fact due to chronic exposure to formaldehyde is damage to muscles and cells of the body which are the leading cause of cancer.[9,10]

Therefore, adsorption and sensor studies of formaldehyde have attracted much attention. In recent years scientists have developed many methods for the sensing of formaldehyde. These mechanisms includes chemical adsorption,[11] catalytic oxidation,[12] physical adsorption,[12] and biotechnical decomposition.[13] By using metal oxides, thermal catalytic oxidation have been performed for sensing of formaldehyde.[14,15] Dirksen *et al.* studied the sensing of formaldehyde by using NiO thin films.[16] Two-dimensional $WO_3$ nanolayers were also explored theoretically as promising candidates for sensing applications especially for HCHO and showing even better performance than graphene and

[a]*Department of Chemistry, COMSATS University, Abbottabad Campus, KPK 22060, Pakistan. E-mail: khurshid@cuiatd.edu.pk; Tel: +92-992-383591*

[b]*Department of Chemistry, College of Science, University of Bahrain, 1051, Bahrain*

† Electronic supplementary information (ESI) available. See DOI: https://doi.org/10.1039/d3ra04019d

borophene.[17] Moreover, metal doped complexes have been used as a sensor. For example, aluminum doped zinc oxide has been employed as a formaldehyde sensor with wide range of sensing ability and of rapid response (8 s) at certain temperature.[18] With all these different types of solid materials have been used explored for sensing applications such as activated carbon, covalent organic framework, graphene, zeolites and metal organic framework.[19,20] These developed mechanisms were not too efficient due to low surface area of adsorbents that are not good enough to adsorb these gases.[21] The other most important drawback of using these adsorbents are that they produce harmful byproducts that are extremely dangerous materials.[14]

Two dimensional (2D) nanomaterials such as covalent organic frameworks (COFs),[22] carbon nitrides ($C_2N$),[23] graphene oxide (GO),[24] and metal–organic frameworks (MOFs)[25] have been extensively used as a sensors because of their large surface to volume ratio consisting of unique electronic properties with extraordinary chemical and physical properties.[26] These materials have been used in many potential applications in opto-electronic, catalysts, energy generation and in storage devices.[27] It is also known that graphene and silicene are employed as electrode materials[28] or electrode additives[29] for applications in batteries. There are many reported mechanisms to improve the catalytic and sensing performance of 2D nanomaterials, such as doping of transition metals and their functionalization.[30,31] Also, these materials have been used as gas sensors. Like, Ma *et al.* reported the sensitivity of small gas molecules such as $NO_2$, CO, $O_2$, and $NH_3$ by palladium doped graphene.[32] It is reported that sensing ability of single walled carbon nanotube could be enhanced by doping of palladium on the SWCNT surface towards $CH_4$, $CH_3OH$ and $SO_2$.[33] The graphene doped with 3d transition metals has been widely studied for sensing applications.[34–36] To increase the sensing abilities of graphene, Ti metal is doped on the surface of graphene for the sensing of $COCl_2$,[37] $NO_2$,[34] CO,[35,38] and HCHO.[39]

In this study we have studied 2D surface, olympicene ($C_{19}H_{12}$) as an effective gas sensor for formaldehyde through density functional theory (DFT). Olympicene has various applications in the field of sensors, high-tech LED's, solar cells and energy storage, sensors devices.[40] Olympicene has been previously investigated as a promising sensor for the detection of chemical warfare agents and toxic industrial gases.[41,42] The geometry of olympicene is composed of five rings out of which four are benzene rings connected like an Olympic ring with two hydrogen atoms extended above and below plane of carbon.[43] Many transition metals such as Ni, Fe and Pd are doped on olympicene to enhance the performance, as a sensor for the detection of formaldehyde. Olympicene commonly originated from pentacene has been recently reported in its stable form.[40,44] From structural properties it is concluded that olympicene can be extensively used in solar cells, LEDs, energy storage devices and in sensor applications.[40,45] In this theoretical study, sensing behavior of transition metal doped olympicene has been studied. Results concluded that TM doped olympicene is excellent adsorbent against formaldehyde. NBO, NCI, QTAIM, EDD analysis has been performed. All stable geometries have been calculated at B3LYP D3 def-2 TZVP level of theory. Also changes in the states have been observed by DOS analysis. To determine the reusability of the olympicene surface recovery time at different temperature are also calculated.

## 2 Computational methodology

All calculations are carried out using ORCA 5.0.1,[46] geometrical optimization is carried out using B3LYP hybrid functional with Grimme dispersion correction D3 and the def2-TZVP basis set.[47] D3 refers to Grimme's D3 dispersion correction, which is commonly used for the evaluation of long-range wander Waal forces. When compared to high-level wavefunction-based benchmarked studies, non-empirical range-separated functionals like LC-BLYP or wB97XD can provide more accurate energies and HOMO–LUMO gaps than B3LYP.[48] The above-mentioned method B3LYP is selected because of its reliable results according to literature. For geometric studies of molecules B3LYP is thought to be an effective parameter. It has been shown in previous studies that B3LYP is an optimal functional to deliver accurate and reliable results with minimum cost.[49] Along with optimization of geometries at B3LYP hybrid functional with Grimme dispersion correction D3 and the def2-TZVP basis set, frequency analysis is also performed at the same level of theory to confirm the true minima nature of the optimized structure on the potential energy surfaces. The absence of negative frequency of the optimized structure confirms that the optimized geometries are at true minima. For analysis of electronic parameters of 2D materials, the B3LYP method is used by the scientific community.[22,50] Therefore, this method is chosen for effective evaluation of natural bond orbital and frontier molecular orbital (FMO) analysis.[51,52] Transition metals are doped on the olympicene surface at different orientations to check their stability. Among all the most stable orientations are further studied as a sensor for formaldehyde. Interaction energies of all stable complexes are calculated through eqn (1).

$$\Delta E_{\text{int}} = E_{\text{complex}} - (E_{\text{analyte}} + E_{\text{TM@OLY}}) \quad (1)$$

where, $E_{\text{complex}}$ is the final interaction energy of the complex, $E_{\text{analyte}}$ is the energy of formaldehyde, and TM@OLY is the energy of the TM@olympicene with formaldehyde. Calculations involving interacting fragments are usually susceptible to basis set superposition error (BSSE). In such complexes, each interacting molecule uses functions from the adjacent molecules which effectively enhances the basis set. Hence, it is necessary to add correction for such errors. In this regard basis set superposition error is an effective approach to reduce the error. Counter poise method corrects this energy as shown in eqn (2).

$$\Delta E_{\text{int, CP}} = \Delta E_{\text{int}} - E_{\text{BSSE}} \quad (2)$$

where $E_{\text{int, CP}}$, is the counterpoised interaction energy, $E_{\text{int}}$ is the raw interaction energy and $E_{\text{BSSE}}$ is energy after basis set superposition error (BSSE) correction.

To evaluate the interaction between TM and olympicene, and between formaldehyde and TM@olympicene, non-covalent interaction analysis is performed with VMD and Multiwfn.[53] Electron density ($\rho$) and reduced density gradient (RDG) are used with the following equation.

$$\mathrm{RDG} = \frac{1}{2(3\pi)^{1/3}} \frac{\nabla\rho}{\rho^{3/4}} \quad (3)$$

The final output files of all the complexes are further evaluated to study non-covalent interactions through NCI and QTAIM analyses *via* Multiwfn software.[53] However their isosurfaces are visualized through VMD.[54]

# 3 Results and discussion

## 3.1 Geometric optimization and interaction energies

DFT calculations are performed to evaluate the performance of olympicene as an efficient electrochemical sensor for sensing of formaldehyde. The optimized geometry of olympicene is shown in the Fig. 1.

Different transition metals are doped on the surface of olympicene. Olympicene surface consists of five benzene rings. These rings provide three different adsorption sites on the top of these rings such as site A, site B, and site C (Fig. 1). Among all, adsorption of metal on site C produces the most stable structure. Basically, five possible bond lengths of olympicene are reported (Fig. 1) which are 1.35 Å (C1–C2), 1.41 Å (C2–C3), 1.40 Å (C3–C4), 1.43 Å (C4–C5), and 1.42 Å (C6–C1). The bonds at the edges where bonded carbons atoms are directly attached with one H-atom show bonds length of 1.35 Å, which is almost comparable to the theoretical ethylenic C–C bond length (1.34 Å) due to structural similarity with ethylene.[55] Similarly, the C–C bond lengths in the interior of olympicene vary from 1.40 Å to 1.43 Å, which is strongly correlated with the reported C–C bond length for graphene (1.42 Å).[56]

Transition metals are checked for stability by optimizing them at different possible spin states such as singlet, triplet, quintet, and septet. The calculated data revealed that Ni is the most stable at triplet spin state, whereas Fe shows stability in quintet state and the most stable spin state for Pd is singlet state. By doping, a little deformation in the geometry of olympicene is observed due to larger difference in atomic radius between transition metals and carbon atom. From different orientations, different interaction energies of Pd@OLY, Ni@OLY, and Fe@OLY are −27.19 kcal mol$^{-1}$, −11.62 kcal mol$^{-1}$, −30.08 kcal mol$^{-1}$ are obtained. Moreover, zero-point energy corrections and basis set superposition error (BSSE) energies are also computed for the considered Pd@OLY, Ni@OLY, and Fe@OLY systems. These all values are reported in Table S1 (ESI).†

The average distance between TM and surface is observed between 2.50 Å to 3.29 Å. Larger distance is observed in the case of iron which is 3.35 Å. While the shortest distance is observed in the case of Pd, that is 2.50 Å. The bond distances and stable complexes of TM@olympicene are reported in Fig. S1 (ESI).† And values of interaction energies and closest interaction distances between interacting atoms are reported in Table S1 (ESI).†

The most stable complexes of transition metal doped surfaces are next evaluated as sensor for formaldehyde. Different orientations are tested with different strong repulsions states, and the most stable orientation with most stable spin state such as triplet (OLY(Ni)/HCHO), quintet (OLY(Fe)/HCHO), and singlet (OLY(Pd)/HCHO) are studied for further analysis. These stable complexes are shown in Fig. 2 and their interaction energies are reported in Table 1. Interaction energies of OLY(Ni)HCHO, OLY(Fe)HCHO, and OLY(Pd)HCHO are −32.35 kcal mol$^{-1}$, −15.98 kcal mol$^{-1}$ and −11.13 kcal mol$^{-1}$ respectively. The highest interaction energy is obtained in the case of OLY(Ni)HCHO that is −32.35 kcal mol$^{-1}$. This highest energy is due to strong forces and efficient overlapping of orbitals of formaldehyde with TM@olympicene. Also, another factor that contributes to their strong interaction is short interaction distance *i.e.*, 1.83 Å between formaldehyde and transition metal. After interaction with formaldehyde,

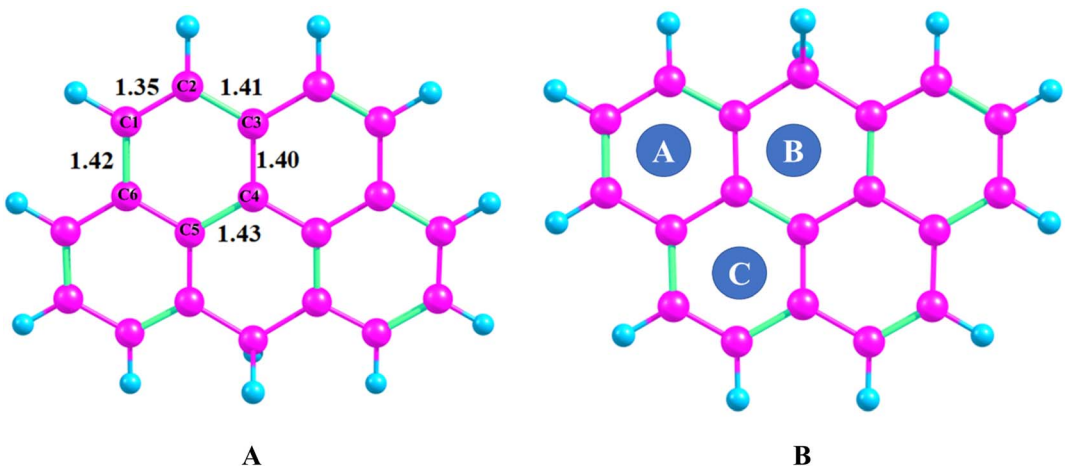


Fig. 1 (A) Optimized geometry of olympicene with individual bond length between carbon (B) different adsorption sites (purple color presents carbon atoms while sky blue is for hydrogen atoms).

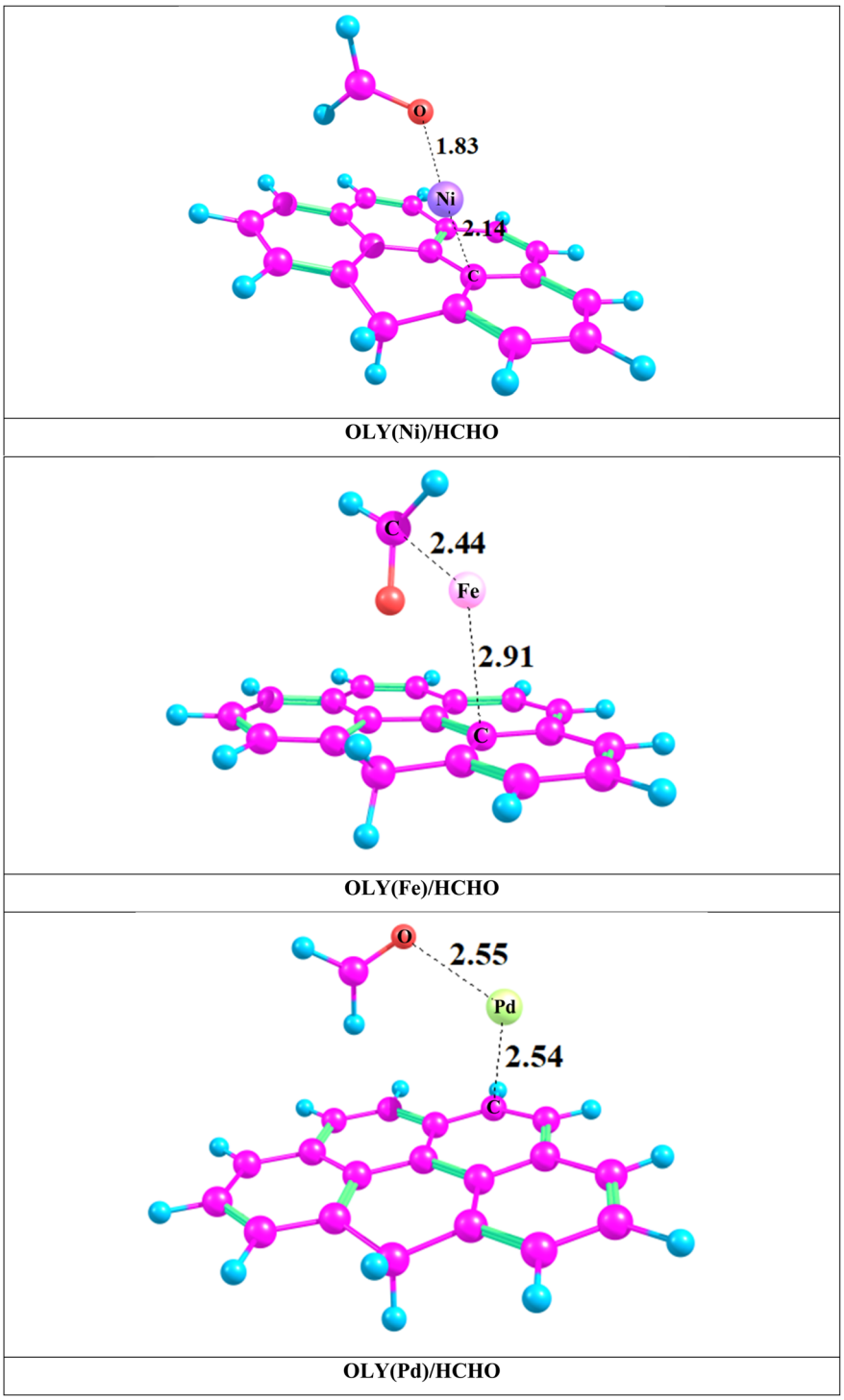


Fig. 2 Stable geometries of OLY(TM)HCHO with shortest intermolecular distances.

interaction distance decreases from 2.68 Å to 2.14 Å (OLY(Ni)/HCHO), and 3.19 Å to 2.91 Å (OLY(Fe)/HCHO). But in case of OLY(Pd)/HCHO, this distance increases by a negligible value *i.e.*, 2.50 Å to 2.54 Å. In general trend, shorter interaction distance indicates higher interaction energy. Therefore, in case of OLY(Ni)/HCHO, the highest interaction energy is strongly correlated with the shortest interaction distance. This trend is consistent with all the stable complexes that are reported. The overall trend of interaction energy is OLY(Ni)/HCHO > OLY(Fe)/HCHO > OLY(Pd)/HCHO. This generally supports physisorption.[23,57,58]

Additionally, basis set superposition error (BSSE) corrected energies as well as BSSE correction energies are also computed for the considered systems (OLY(Ni)/HCHO, OLY(Fe)/HCHO

Table 1 Interaction energies, BSSE corrected energy, BSSE correction energy and intermolecular bond (Å) distances of stable complexes

| Complexes | Interaction energy ($E_{in}$) (kcal mol$^{-1}$) | BSSE corrected energy (kcal mol$^{-1}$) | BSSE correction energy (kcal mol$^{-1}$) | $D_{int}$ of TM and FMH | $D_{int}$ of TM and OLY |
|---|---|---|---|---|---|
| OLY(Ni)/HCHO | −32.59 | −31.67 | 0.93 | 1.83 | 2.14 |
| OLY(Fe)/HCHO | −15.98 | −15.39 | 0.59 | 2.44 | 2.91 |
| OLY(Pd)/HCHO | −11.13 | −10.41 | 0.72 | 2.55 | 2.54 |
| OLY(Ti)/HCHO | −48.72 | −47.83 | 0.89 | — | — |

and OLY(Pd)/HCHO). The results in Table 1 indicates that BSSE corrected energies follow the same trend as in the case of interaction energy *i.e.*, OLY(Ni)/HCHO > OLY(Fe)/HCHO > OLY(Pd)/HCHO. The highest interaction energy observed for OLY(Ni)/HCHO complex is strongly correlated with the highest BSSE corrected energy. The calculated BSSE correction energies also justify the correlation of interaction energies with the BSSE corrected energies for all studied complexes (OLY(Ni)/HCHO, OLY(Fe)/HCHO and OLY(Pd)/HCHO). Additionally, OLY(Ti)/HCHO complex is also considered for comparison. Higher interaction and BSSE corrected energies are observed in the case of OLY(Ni)/HCHO complex as compared to other studied complexes.

# 4 Electronic properties

To evaluate the nature of interaction between formaldehyde and TM@olympicene, different electronic properties such as natural bond orbital (NBO), frontier molecular orbital (FMOs), density of states (DOS) and electron density differences (EDD) analyses are performed.

## 4.1 FMO analysis

Conductivity of the sensor is evaluated through FMO analysis. The electronic properties are used to evaluate the conductivity and resistivity of the sensor. HOMO–LUMO gap of bare olympicene, transition metal doped olympicene and final complexes are reported in Table 2, and orbital densities are reported in Fig. S2 (ESI).† The highest occupied molecular orbital has the ability to donate the electrons, whereas, lowest unoccupied molecular orbitals has the ability to accept electron.[59] After interaction of formaldehyde with TM doped olympicene, certain changes in electronic properties are observed. As mentioned earlier, this change in the electronic properties is due to the change in the energy gap. The increase in the gap results in the higher resistivity while higher conductivity is associated with reduction in the band gap.

The energies of HOMO and LUMO of bare olympicene are −5.51 eV and −1.49 eV, respectively and their corresponding energy gap is 4.01 eV. On adsorption of transition metals on the surface, a reduction in the gap is observed. The energy gaps are 2.14 eV (Ni@OLY), 2.90 eV (Fe@OLY), and 2.99 eV (Pd@OLY). From results is concluded that the highest reduction is observed in the case of Ni@OLY. As we know that, conductivity of the sensor is increased when the band gap is reduced.[60]

After interaction of formaldehyde with transition metal doped olympicene a clear reduction in the $E_{H\text{-}L}$ is observed. $E_{H\text{-}L}$ gaps are reduced to 1.16 eV (OLY(Ni)/HCHO), 2.54 eV (OLY(Fe)/HCHO), and 2.91 eV (OLY(Pd)/HCHO) from 2.14 eV (Ni@OLY), 2.90 eV (Fe@OLY), and 2.99 eV (Pd@OLY). Among all complexes, the highest reduction in the band gap is observed in the case of OLY(Ni)/HCHO. It is well known that greater band gap reduction results in more conductivity.[60] Based on FMO results, the highest conductivity is observed in case of Ni doped complex among all studied complexes.

To understand the interaction mechanism, it is important to observe the orbital densities of TM@olympicene and TM@olympicene with formaldehyde. Both HOMO and LUMO isosurfaces of olympicene are evenly distributed over all the surfaces. But in case of transition metal doped olympicene, the density is shifted towards transition metals. However, in all three complexes the density of both HOMO and LUMO is slightly different. In OLY(Fe)/HCHO density is shifted to the surface while, in case of OLY(Ni)/HCHO density of HOMO is totally shifted

Table 2 The energies of LUMO, HOMO, band gap (eV), and NBO charges for all TM@OLY and OLY(TM)/HCHO complexes calculated at B3LYP D3 Def-2 TZVP level of theory and wB97XD-D3 Def-2 TZVP level of theory

| | B3LYP | | | wB97XD | | | |
|---|---|---|---|---|---|---|---|
| Complexes | $E_{HOMO}$ (eV) | $E_{LUMO}$ (eV) | $E_{H-L}$ gap (eV) | $E_{HOMO}$ (eV) | $E_{LUMO}$ (eV) | $E_{H-L}$ gap (eV) | $Q_{NBO}$ (HCHO) |
| OLY | −5.51 | −1.49 | 4.01 | −7.52 | 0.30 | 7.82 | — |
| Pd@OLY | −4.81 | −1.81 | 2.99 | −7.02 | 0.23 | 7.25 | — |
| Ni@OLY | −3.88 | −1.74 | 2.14 | −5.53 | −0.02 | 5.51 | — |
| Fe@OLY | −4.62 | −1.70 | 2.90 | −6.74 | 0.04 | 6.79 | — |
| OLY(Ni)/HCHO | −3.05 | −1.89 | 1.16 | −4.58 | −0.40 | 4.18 | 0.104 |
| OLY(Fe)/HCHO | −4.16 | −1.63 | 2.54 | −5.91 | 0.14 | 6.05 | −0.225 |
| OLY(Pd)/HCHO | −4.59 | −1.67 | 2.91 | −6.77 | 0.18 | 6.95 | 0.016 |

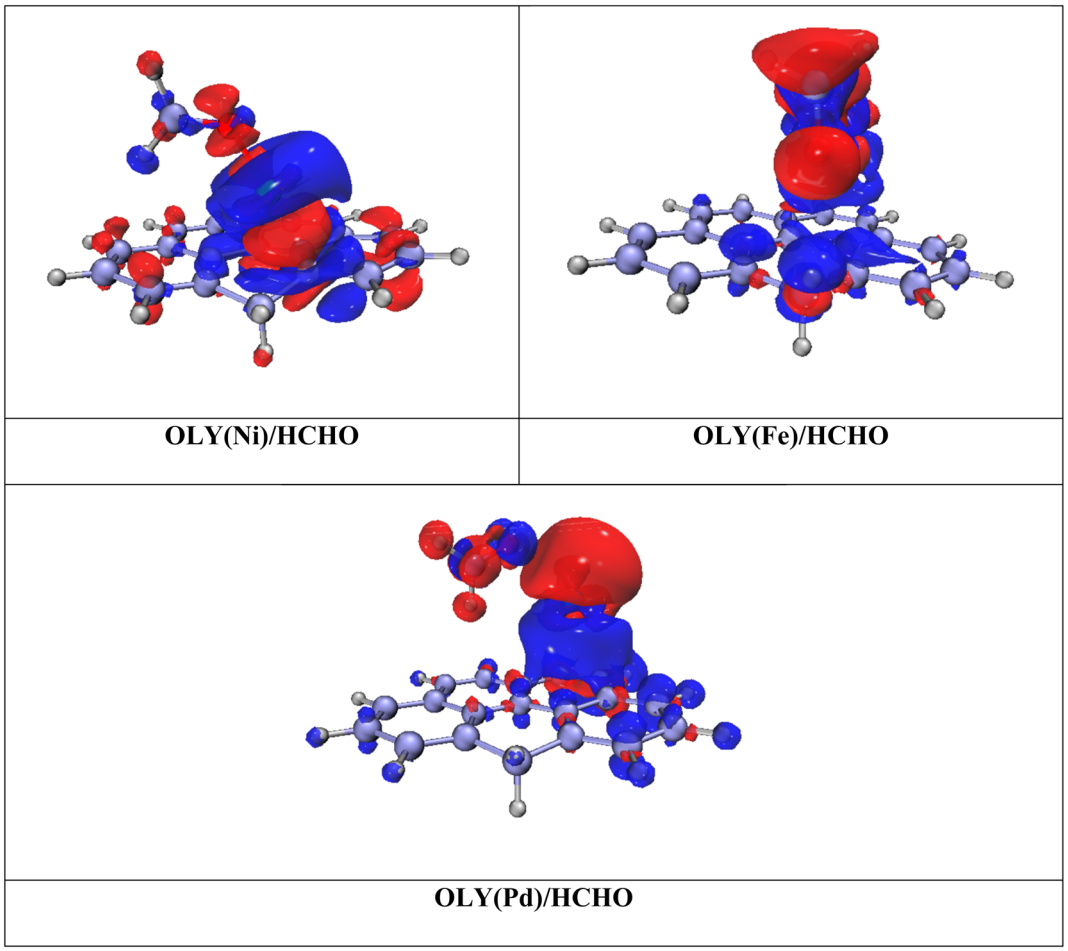


Fig. 3 Electron density difference (EDD) plots of OLY(TM)/HCHO complexes.

towards formaldehyde, the third case OLY(Pd)/HCHO is also exactly like OLY(Ni)/HCHO. So, results concluded that the electrons are transferred from surface to analyte due to which a clear decrease in the band gap is observed which results in higher interaction between surface and analyte.

All transition metals have positive charge except Fe after interaction with olympicene, which indicates that charges are being transferred from transition metals to olympicene. It is also observed that density is shifted from transition metal to formaldehyde and concluded that both surface and transition metals transfer electron to the analyte. These results are also consistent with the NBO analysis (Table 2).

Moreover, in addition to B3LYP D3 Def-2 TZVP level of theory, electronic properties of the studied systems are also computed at wB97XD-D3 Def-2 TZVP level of theory (see Table 2). The values of HOMO, LUMO and energy gaps vary depending on used functional. However, the trend of energy gaps upon metal adsorption as well as upon complexation with formaldehyde is same with that of B3LYP. In both cases, the highest reduction in energy gap upon metal adsorption is seen for Ni@OLY. Similarly, for interaction of formaldehyde the highest reduction in energy gap is also noticed for OLY(Ni)/HCHO complex.

### 4.2 Density of state (DOS) analysis

To examine the conductivity response of the sensor, it is most important to study the interaction mechanism between surface (TM@olympicene) and analyte (formaldehyde). Conductivity is often referred to as the transferring of electron from valence band to the conduction band. And between these two, there lies a Fermi level. Therefore, we can say that in the conduction mechanism electrons play a pivotal role. To study the conduction mechanism, DOS analysis of TM@OLY and OLY(TM)/HCHO complexes is performed and reported in Fig. S6 (ESI).†

From spectra, it is concluded that the $E_{HOMO}$ and $E_{LUMO}$ of bare olympicene are −5.51 eV and −1.49 eV respectively, whereas their band gap appears at 4.01 eV. On interaction of olympicene with the TM a certain reduction in the band gap is observed *i.e.*, it is shifted from 4.01 eV to 2.99 eV (Pd@OLY), 2.14 eV (Ni@OLY), and 2.90 eV (Fe@OLY). Now, on interaction of TM@OLY to the formaldehyde, this energy gap is further reduced. For example, energy gap is reduced from 2.14 eV to 1.16 eV in case of OLY(Ni)/HCHO, 2.90 eV to 2.54 eV (OLY(Fe)/HCHO), and 2.99 eV to 2.91 eV in (OLY(Pd)/HCHO). On formation of these virtualized energy levels on interaction with formaldehyde results in the reduction of energy gap, which in return increase the conductivity of the sensor. Hence, DOS

spectrum clearly indicates the reduction of energy gap with the interaction of TM@OLY with the formaldehyde.

### 4.3 Natural bond orbital (NBO) and electron density difference (EDD) analysis

NBO and EDD analyses mainly determine the magnitude of charge transfer between surface and analyte. To get an insight about the magnitude of charge transfer, NBO analysis is performed while for visualization of results, EDD analysis is performed.

NBO charge analysis is performed to study the charge transfer between surface and analyte. Charge transfer values in the case of OLY(Pd)/HCHO and OLY(Ni)/HCHO are positive, 0.016 and 0.104 respectively. This indicates that charges are being transferred from analyte to the surface. While for OLY(Fe)/HCHO, the results are totally different. The value obtained is negative (−0.225) which shows the charge transfer from surface to analyte. In the case of OLY(Ni)/HCHO the amount of charge transfer is highest so as the interaction energy is highest for this complex. Also, in case of OLY(Pd)/HCHO charge is transferred to the olympicene because of presence of electron rich oxygen atom on formaldehyde. NBO charges are reported in Table 2.

To visualize the charge transfer EDD analysis is performed. The Iso-surfaces of all stable complexes OLY(TM)HCHO are shown in Fig. 3. Iso-surface shows two different colors red and blue. Blue color show accumulation of charges, this accumulation is mainly due to the presence of highly electron rich benzene rings of olympicene. While depletion of electronic density is mainly shown by red color density. The presence of two different types of colors confirms the charge transfer between surface and analyte. Electron density difference in the case of OLY(Pd)/HCHO clearly indicates that electron is being transferred from TM@olympicene to the formaldehyde. While for OLY(Fe)/HCHO and OLY(Ni)/HCHO all density is shifted towards olympicene. These all results are consistent with the results of NBO analysis.

### 4.4 NCI analysis

To get a deep insight on the nature of interactions present, noncovalent interaction (NCI) analysis is performed. It consists of 2D, and 3D iso-surfaces, as shown in Fig. 4. RDG spectra shown consist of three different colors (blue, green, and red). These three different colors show three types of forces present between surface and analytes. Blue color represents strong attractive forces such as hydrogen bonding. Green color shows weak forces such as London dispersion forces, while red color represent steric repulsion between interacting species.[61] If we look at the 3D plots, the intensity of the iso surface is directly related to the interaction, greater the intensity greater will be the strength of interacting forces present.

Green patches appear between analyte and the olympicene in case of OLY(Fe)/HCHO and OLY(Pd)/HCHO. This is the confirmation of presence of weak forces between surface and analyte. While, in these two complexes red patches also appear between surface and analyte, and between the benzene rings of olympicene. This shows that steric repulsion also presents between surface and analyte and between the rings of the surface. In case of OLY(Ni)/HCHO, intensity of patches between surface and analyte is very less, which is the indication of presence of weak dispersive forces, but here blue patches indicate the confirmation of strong hydrogen bonded forces (see Fig. 4).

The 2D NCI graph is plotted between sign($\lambda_2$) $\rho$ (a.u.) on $x$-axis while on $y$-axis reduced density gradient (RDG) is plotted. Here three different colors red, green, and blue also represent repulsive interactions, weak van der Waals forces, and strong hydrogen bonding, respectively. Sign($\lambda_2$) (more negative) on $x$-axis shown the strong forces such as electrostatic interaction and hydrogen bonding. Between 0.00 au, and −0.01 au, indicates the presence of strong electrostatic interaction. 2D NCI graphs shown that red and green spikes represent strong electrostatic interaction between surface and analyte. Intensity of green spikes in OLY(Fe)/HCHO show weak van der Waals forces as compared to other two complexes. The 3D isosurfaces shown in Fig. 4 reveal that the presence of mixture of red and blue spikes in the case of OLY(Ni)/HCHO and OLY(Pd)/HCHO between metal and olympicene surface, which shows steric repulsions and hydrogen bonding, respectively. Similarly, in the case of OLY(Fe)/HCHO, these isosurfaces appear at the interacting site of Fe and HCHO. These results are also justified from the red spikes appearing in the 2D RDG spectra (see Fig. 4). These results are consistent with interaction energy analysis.

### 4.5 QTAIM analysis

Non-covalent interactions are further evaluated by quantum theory of atoms in molecules (QTAIM) analysis. Types and structure of bonds are examine by QTAIM which was proposed by Bader *et al.*[62] The theory is used to analyze bond critical points (BCPs). This theory helps in determining individual bond interaction energy through total energy density (H(r)), potential energy density ($V(r)$), kinetic energy density ($G(r)$), Laplacian of the charge density ($\nabla 2\ \rho$), and total electron density ($\rho$) at bond critical point. Intermolecular interactions determined based on these points are reported in Table S2 (ESI†) and critical points are shown in Fig. 5. In case of hydrogen bonding the electron density should be greater than 1 ($\rho > 1$), while in case of weak interactions, the electronic density value should be less than one ($\rho < 1$). It is observed that, at bond critical point the potential energy density value is always negative while $G(r)$ is always positive. If the value of $H(r)$ is less than zero, then it means covalent interactions are present and if the values are greater than zero then non-covalent interactions are present. The total bond critical points observed in studied HCHO/(TM) OLY complexes are 2 (HCHO/(Ni)OLY), 2 (HCHO/(Fe)OLY) and 2 (HCHO/(Pd)OLY) through QTAIM analysis. For BCPs explanation following equations can be used,

$$\frac{1}{4}\nabla 2\rho(r) = 2G(r) + V(r) \quad (4)$$

$$H(r) = G(r) + V(r) \quad (5)$$

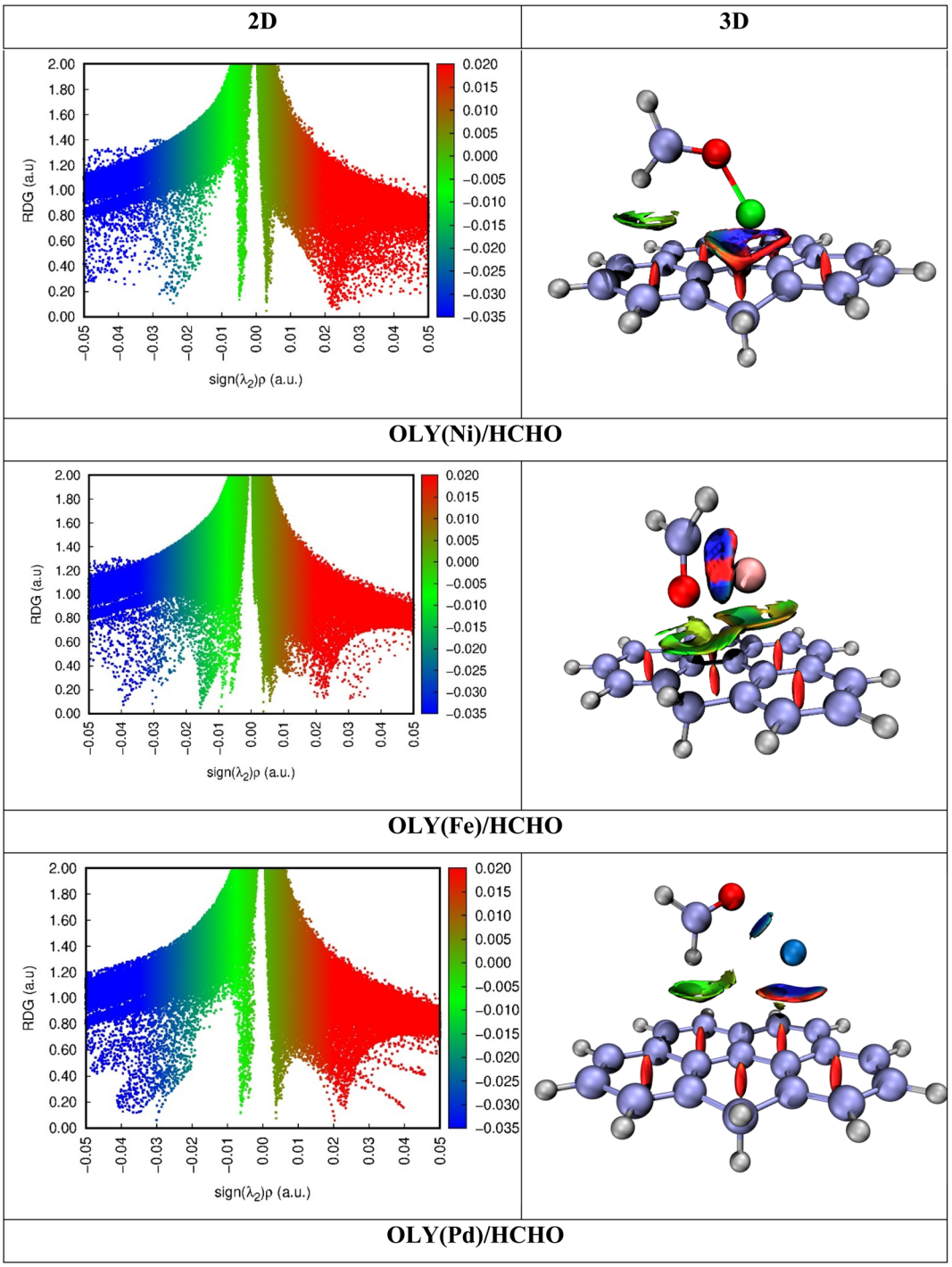


Fig. 4 2D RDG scatter map and 3D iso-surfaces of HCHO/(TM)OLY complexes.

From values of Laplacian of electron density, it is seen that for HCHO/(Ni)OLY and HCHO/(Pd)OLY complexes, high values of 0.666 and 0.108 a.u. are observed, respectively. Also remaining BCPs are in accordance with the Laplacian value. Which is the clear indication to the presence of non-covalent interactions. Moreover, it is further observed that the value of electron density is less than 0.1 ($\rho < 0.1$), which is the clear indication of the presence of van der Waals interactions. As all the values of electron densities and Laplacian electron densities are positive in all cases of HCHO/(TM)OLY complexes, these all-positive values indicate the presence of non-covalent interaction, which are in accordance with the NCI analysis performed. Apart from this discussion the nature of interactions is also indicated by the ratio −V/G. If −V/G is less than zero, then it means that non-covalent interactions are present. In all complexes at one point

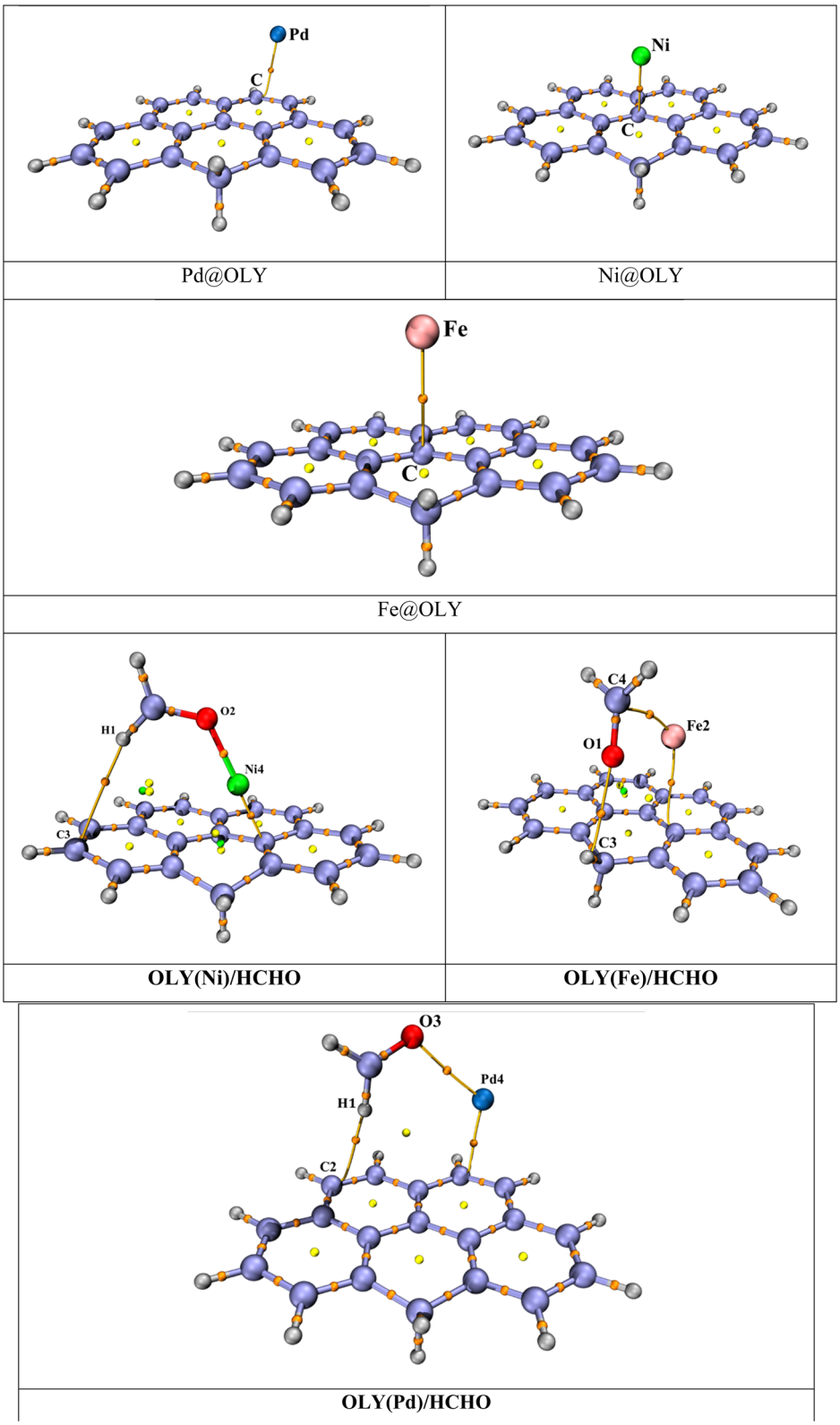


Fig. 5 Iso-surfaces of all complexes (OLY(TM)/HCHO) in QTAIM analysis.

between transition metal and formaldehyde the value of −V/G is greater than zero, which means that covalent interaction is present between formaldehyde and transition metal. While at other point between formaldehyde and olympicene this value decreased down to less than zero which confirms the non-covalent interactions.

## 5 Recovery response time

By recovery response time of a sensor, we can generate the idea about the reliability and the sensitivity of the sensor. By thermal effect and theoretical studies, we calculated the recovery time at different temperatures with the help of transition state theory at different temperatures (298, 350, and 400 K). eqn (6) can be used for this purpose.

$$\tau = \upsilon^{-1} \exp\left(\frac{-E_{ads}}{kT}\right) \quad (6)$$

Here, $T$ represent the temperature of the system, $k$ shows the Boltzmann constant with the value of $8.62 \times 10^{-5}$ eV $K^{-1}$, $\upsilon$ denotes the attempt frequency, the attempt used here is for $NO_2$ molecule ($10^{12}$ $s^{-1}$).[63] From above mentioned equation recovery time is calculated at three different temperatures 298 K, 350 K, and 400 K and are reported in Table S3 (ESI).† The observed recovery times at 400 K are $1.4 \times 10^{-4}$ s (OLY(Ni)/HCHO), $4.2 \times 10^{-6}$ s (OLY(Fe)/HCHO), and $2.55 \times 10^{-7}$ s (OLY(Pd)/HCHO). From the trend it is observed that as the temperature is decreased the recovery response time is also decreased. At 400 K the desorption period for $NO_2$ and $H_2S$ is 115 s and 28 s respectively.[64] According to eqn (6), there is a direct relation between adsorption energy and recovery time, complexes with the highest interaction energy leads to increase in the recovery time of the sensor. Similarly, complexes with least adsorption energy, their recovery response time is automatically reduced. With obtained results it is concluded that at room temperature (298 K) the recovery response is higher, which proves olympicene as a good adsorbent material for formaldehyde.

## 6 Conclusions

The adsorption behavior of formaldehyde on transition metal doped olympicene is analyzed by DFT studies at B3LYP-D3 def-2/TZVP level of theory. At first the most stable spin state was obtained. Calculations are performed at different orientations from which the complexes with highest interaction energies are reported. OLY(Ni)/HCHO has the highest interaction energy apart from other two, while OLY(Pd)/HCHO has the lowest energy. From QTAIM and NCI analysis it is observed that non-covalent interactions are present between TM@olympicene and formaldehyde. The results of QTAIM further revealed that all electron density values are less than 0.1 which shows the presence of weak van der Waals forces. From NCI analysis, 3D iso-surfaces depicts that strong forces are present in OLY(Fe)/HCHO and OLY(Pd)/HCHO as compared to the OLY(Ni)/HCHO. FMO results indicate a decrease in energy gap of complexes upon interaction with formaldehyde. NBO analysis confirm that charges are being transferred from TM@olympicene to formaldehyde in case of OLY(Fe)/HCHO. While in OLY(Pd)/HCHO and OLY(Ni)/HCHO complexes, charge is transferred from formaldehyde to TM@olympicene. The results of NBO are further evaluated through EDD analysis in which transfer of charges have been observed through visualization. Overall, OLY(Ni)/HCHO complex showed the strong interaction with formaldehyde, hence declare as the most selective sensor for the efficient detection of formaldehyde.

## Conflicts of interest

There are no conflicts to declare.

## References

1 J. Chakraborty, *Ann. Am. Assoc. Geogr.*, 2009, **99**, 674–697.
2 D. Irving, S. Wijffels and J. Church, *Geophys. Res. Lett.*, 2019, **46**, 4894–4903.
3 T. Salthammer, *Angew. Chem., Int. Ed.*, 2013, **52**, 3320–3327.
4 W. C. Krauss, *Trans. Am. Microsc. Soc.*, 1896, **17**, 315–318.
5 T. Salthammer, S. Mentese and R. Marutzky, *Chem. Rev.*, 2010, **110**, 2536–2572.
6 P.-R. Chung, C.-T. Tzeng, M.-T. Ke and C.-Y. Lee, *Sensors*, 2013, **13**, 4468–4484.
7 V. J. Cogliano, Y. Grosse, R. A. Baan, K. Straif, M. B. Secretan, F. E. Ghissassi and Working Group for Volume 88, *Environ. Health Perspect.*, 2005, **113**, 1205–1208.
8 S. Shao, H. W. Kim, S. S. Kim, Y. Chen and M. Lai, *Appl. Surf. Sci.*, 2020, **516**, 145932.
9 Y. Wang, Y. Zhou and Y. Wang, *Sens. Actuators, B*, 2020, **323**, 128695.
10 W. H. Organization, *WHO guidelines for indoor air quality: selected pollutants*, World Health Organization. Regional Office for Europe, 2010.
11 S. Srisuda and B. Virote, *J. Environ. Sci.*, 2008, **20**, 379–384.
12 H. Wang, Z. Wu, W. Zhao and B. Guan, *Chemosphere*, 2007, **66**, 185–190.
13 W. Chen, J. S. Zhang and Z. Zhang, *ASHRAE Trans.*, 2005, **111**, 1101–1114.
14 H.-X. Ding, A.-M. Zhu, X.-F. Yang, C.-H. Li and Y. Xu, *J. Phys. D: Appl. Phys.*, 2005, **38**, 4160.
15 D. Huixian, Z. Aimin, Y. Xuefeng, L. Cuihong and X. Yong, *J. Phys. D: Appl. Phys.*, 2005, **38**, 4160.
16 J. A. Dirksen, K. Duval and T. A. Ring, *Sens. Actuators, B*, 2001, **80**, 106–115.
17 J.-H. Li, J. Wu and Y.-X. Yu, *Appl. Surf. Sci.*, 2021, **546**, 149104.
18 N. Choi, H. Lee, S. Moon and W. Yang, *Sens. Actuators, B*, 2012, **175**, 132–136.
19 K. Saadat and H. Tavakol, *RSC Adv.*, 2015, **5**, 55227–55237.
20 H. Tavakol, F. Hashemi and M. R. Molavian, *Struct. Chem.*, 2017, **28**, 1687–1695.
21 J. Mo, Y. Zhang, Q. Xu, Y. Zhu, J. J. Lamson and R. Zhao, *Appl. Catal., B*, 2009, **89**, 570–576.
22 S. Sarfaraz, M. Yar and K. Ayub, *Mater. Sci. Semicond. Process.*, 2022, **139**, 106334.
23 S. Sarfaraz, M. Yar, A. A. Khan, R. Ahmad and K. Ayub, *J. Mol. Liq.*, 2022, **352**, 118652.
24 V. S. Bhati, M. Kumar and R. Banerjee, *J. Mater. Chem. C*, 2021, **9**, 8776–8808.
25 S.-J. Choi and I.-D. Kim, *Electron. Mater. Lett.*, 2018, **14**, 221–260.
26 Y. Li, W. Gao, L. Ci, C. Wang and P. M. Ajayan, *Carbon*, 2010, **48**, 1124–1130.

27 M. Wang, L. Chen, J. Zhou, L. Xu, X. Li, L. Li and X. Li, *J. Mater. Sci.*, 2019, **54**, 483–492.
28 Y.-X. Yu, *J. Phys. Chem. C*, 2019, **123**, 205–213.
29 Y.-X. Yu, *ACS Appl. Mater. Interfaces*, 2014, **6**, 16267–16275.
30 L. Ma, J.-M. Zhang, K.-W. Xu and V. Ji, *Appl. Surf. Sci.*, 2015, **343**, 121–127.
31 W. Xiao, R. Zeng, L. Cheng, J. Wang, L. Jiang and L. Wang, *RSC Adv.*, 2015, **5**, 61861–61867.
32 G. Gao, Y. Jiao, F. Ma, Y. Jiao, E. Waclawik and A. Du, *J. Phys. Chem. C*, 2015, **119**, 13124–13128.
33 X. Zhou, W. Q. Tian and X.-L. Wang, *Sens. Actuators, B*, 2010, **151**, 56–64.
34 M. Zhou, Y.-H. Lu, Y.-Q. Cai, C. Zhang and Y.-P. Feng, *Nanotechnology*, 2011, **22**, 385502.
35 Y. Li, X. Sun, L. Zhou, P. Ning and L. Tang, *J. Mol. Model.*, 2019, **25**, 1–12.
36 L. B. Shi, Y. P. Wang and H. K. Dong, *Appl. Surf. Sci.*, 2015, **329**, 330–336.
37 T. Zhang, H. Sun, F. Wang, W. Zhang, S. Tang, J. Ma, H. Gong and J. Zhang, *Appl. Surf. Sci.*, 2017, **425**, 340–350.
38 N. Promthong, C. Tabtimsai, W. Rakrai and B. Wanno, *Struct. Chem.*, 2020, **31**, 2237–2247.
39 X. Chen, L. Xu, L.-L. Liu, L.-S. Zhao, C.-P. Chen, Y. Zhang and X.-C. Wang, *Appl. Surf. Sci.*, 2017, **396**, 1020–1025.
40 A. Mistry, B. Moreton, B. Schuler, F. Mohn, G. Meyer, L. Gross, A. Williams, P. Scott, G. Costantini and D. J. Fox, *Chem.–Eur. J.*, 2015, **21**, 2011–2018.
41 U. Sohail, F. Ullah, T. Mahmood, S. Muhammad and K. Ayub, *ACS Omega*, 2022, **7**, 18852–18860.
42 U. Sohail, F. Ullah, T. Mahmood and K. Ayub, *Mater. Sci. Semicond. Process.*, 2022, **144**, 106620.
43 N. P. Tsvetkov, E. Gonzalez-Rodriguez, A. Hughes, G. dos Passos Gomes, F. D. White, F. Kuriakose and I. V. Alabugin, *Angew. Chem.*, 2018, **130**, 3713–3717.
44 A. J. Valentine and D. A. Mazziotti, *J. Phys. Chem. A*, 2013, **117**, 9746–9752.
45 E. Shakerzadeh, *Monatsh. Chem.*, 2019, **150**, 1745–1751.
46 F. Neese, F. Wennmohs, U. Becker and C. Riplinger, *J. Chem. Phys.*, 2020, **152**, 224108.
47 P. Lykos and G. Pratt, *Rev. Mod. Phys.*, 1963, **35**, 496.
48 N. Mardirossian and M. Head-Gordon, *J. Chem. Phys.*, 2016, **144**, 214110.
49 A. S. Rad and K. Ayub, *J. Mol. Liq.*, 2017, **238**, 303–309.
50 L. N. Anderson, M. B. Oviedo and B. M. Wong, *J. Chem. Theory Comput.*, 2017, **13**, 1656–1666.
51 A. S. Rad and K. Ayub, *Vacuum*, 2016, **131**, 135–141.
52 M. Kamran, H. Ullah, A. S. Anwar-ul-Haq, S. Bilal, A. A. Tahir and K. Ayub, *Polymer*, 2015, **72**, 30–39.
53 T. Lu and F. Chen, *J. Comput. Chem.*, 2012, **33**, 580–592.
54 Y. Lu, Z. Lan and W. Thiel, *J. Comput. Chem.*, 2012, **33**, 1225–1235.
55 A. Cassuto, M. Mane, J. Jupille, G. Tourillon and P. Parent, *J. Phys. Chem.*, 1992, **96**, 5987–5993.
56 R. Gholizadeh and Y.-X. Yu, *J. Phys. Chem. C*, 2014, **118**, 28274–28282.
57 Y. S. Al-Faiyz, S. Sarfaraz, M. Yar, S. Munsif, A. A. Khan, B. Amin, N. S. Sheikh and K. Ayub, *Nanomaterials*, 2023, **13**, 251.
58 M. Aetizaz, S. Sarfaraz and K. Ayub, *J. Mol. Liq.*, 2023, **369**, 120955.
59 M. Aetizaz, S. Sarfaraz and K. Ayub, *J. Mol. Liq.*, 2022, 120955.
60 H. Sajid, T. Mahmood and K. Ayub, *Synth. Met.*, 2018, **235**, 49–60.
61 H. Ullah, A.-u.-H. A. Shah, S. Bilal and K. Ayub, *J. Phys. Chem. C*, 2013, **117**, 23701–23711.
62 R. Bader, T. Nguyen-Dang and Y. Tal, *Rep. Prog. Phys.*, 1981, **44**, 893.
63 J. Beheshtian, M. T. Baei, A. A. Peyghan and Z. Bagheri, *J. Mol. Model.*, 2012, **18**, 4745–4750.
64 S. Ma, L. Su, L. Jin, J. Su and Y. Jin, *Phys. Lett. A*, 2019, **383**, 125868.